Supporting Information: Directional excitation of a high-density magnon gas using coherently driven spin waves

Brecht G. Simon[1,†], Samer Kurdi[1,†], Helena La[1], Iacopo Bertelli[1,2], Joris J. Carmiggelt[1], Maximilian Ruf[3], Nick de Jong[3,4], Hans van den Berg[3,4], Allard J. Katan[1], Toeno van der Sar[1,*]

Affiliations

[1]Department of Quantum Nanoscience, Kavli Institute of Nanoscience, Delft University of Technology, 2628 CJ, Delft, The Netherlands
[2]Huygens-Kamerlingh Onnes Laboratorium, Leiden University, 2300 RA, Leiden, The Netherlands
[3]QuTech, Delft University of Technology, 2628 CJ, Delft, The Netherlands
[4]Netherlands Organisation for Applied Scientific Research (TNO), 2628 CK Delft, The Netherlands

[†] These authors contributed equally to this work.
[*] Corresponding author. Email: t.vandersar@tudelft.nl

1 YIG Sample

We study a 235 ± 10 nm thick film of (111)-oriented ferrimagnetic insulator yttrium iron garnet (YIG) grown on a gadolinium gallium garnet substrate by liquid-phase epitaxy (Matesy GmbH). The stripline (length of 2 mm, width of 30 µm, and thickness of 200 nm) used for spin-wave excitation was fabricated directly on the YIG surface using e-beam lithography, using a double layer PMMA resist (A8 495K / A3 950K) and a top layer of Elektra95, followed by the deposition of 5 nm / 200 nm of Cr/Au.

2 Measurement setup

Our scanning NV-magnetometry setup is equipped with two stacks of Attocube positioners (ANPx51/RES/LT) and scanners (ANSxy50/LT and ANSz50/LT) that allow for individual positioning of the tip and sample. We first position the NV tip in the focus point of the objective (LT-APO/VISIR/0.82) and use the scanners of the sample stack to create spatial PL images (lateral and height). To record the NV PL, we use our home-built confocal setup, which is equipped with a 515 nm green laser (Cobolt 06-MLD, pigtailed) for NV excitation. We use a fiber collimator (Schäfter+Kirchhoff 60FC-T) to couple the laser out into free space. A dichroic mirror (Semrock Di03-R532-t3-25x36) is used to reflect the green laser, which is then focused by the objective lens (LT-APO/VISIR/0.82) on the tip of a homemade all-diamond cantilever probe (Supporting Information Note 3). The shape of the tip aides the guiding of the NV PL back towards the objective where it is collimated and transmitted by the dichroic mirror and additionally filtered by a long-pass filter (BLP01-594R-25) before it is focused on the chip of an avalanche photodiode (APD) (Excelitas SPCM-AQRH-13). The resulting signal is collected and counted by a National Instruments DAQ card. A SynthHD (v2) dual channel microwave generator (Windfreak Technologies, LLC) is used for driving the NVs and exciting the spin waves. High-speed pulse sequences are generated by a PulseBlasterESR-PRO pulse generator (SpinCore Technologies, Inc.).

3 Diamond tip fabrication

3.1 NV implantation

Our scanning tip is fabricated from a (001)-oriented electronic grade type IIa diamond grown via chemical vapor deposition by Element 6. The diamond is laser cut and polished (Almax EasyLab) into 2x2x0.05 mm^3 chips and subsequently cleaned in fuming nitric acid. To remove surface damage from the polishing [1], we use inductively coupled plasma reactive ion etching (ICP-RIE) to remove the top 5 µm. The diamond is implanted with 15N ions at 6 keV with a dose of 10^{13} ions/cm^2 by INNOViON. After implantation, we clean the samples in a tri-acid solution (H_2SO_4:$HClO_4$: HNO_3 = 1:1:1) at 120 °C for 1 hour. We then anneal the diamond for 8 hours at 800 °C at approximately 10^{-6} mbar, followed by another cleaning step in a tri-acid solution.

3.2 Structuring diamond

To structure the diamond into a scanning tip and for mounting this tip in our AFM setup, we follow Refs. [1, 2]. We first thin down the ∼45 µm thick diamond to ∼5-7 µm in a 1.2x1.2 mm^2 area in the center [1, 3]. The diamond is then flipped with the NV side facing up and glued (with PMMA) to a silicon carrier wafer to enable spin coating. An 40-50 nm titanium etch mask is deposited using RF-magnetron sputtering and a layer of about 800 nm PMMA (950K A8) is spin coated and patterned using e-beam lithography into 20x50 $µm^2$ rectangular masks. The mask is then transferred into the titanium using SF6/He plasma RIE. Subsequently, an anisotropic oxygen etch transfers the cantilevers into the diamond with a thickness of about 3 µm [1, 3]. We clean the sample using hexafluoride (40%, HF) and deposit a new layer of 5 nm of titanium to improve the adhesion of the FOx-16 resist that we spincoat subsequently and which serves as the etch mask for the 1.5 µm tall diamond pillars that are created in a final anisotropic oxygen etch. The resulting tips have a diameter of approximately 300 nm and therefore contain about 100 NVs at 20 nm below its apex. The diamond is cleaned to get rid of the titanium/FOx mask in HF and in fuming nitric acid (100%) to remove possible organic contaminants. Finally, the diamond tip is glued (UV glue) to the end of a pulled optical fibre that is connected to a tuning fork for AFM operation[1].

4 Magnetic field calibration

In our experiments we apply the magnetic external field $\vec{B}_0$ using a permanent magnet (S-10-20-N, Supermagnete) onto a linear translation stage (MTS25-Z8, Thorlabs, controlled by a KDC101 Thorlabs servo motor). To vary the strength of the external field, we change the position of the stage to bring the magnet closer to the sample and tip. We orient

the magnet in such a way that the field aligns with one of the four NV families[i] (which is $54.7 \pm 1.8°$ with respect to the normal of the YIG surface) and to magnetize the YIG film along the length of the stripline. At each magnetic field, we calibrate its magnitude and orientation by measuring the eight ESR frequencies $f_{i=1-8}$ of the four NV families(NV_{1-4}) (Fig. 1b, main text). From these frequencies we determine $\vec{B}_0$ by performing a least square minimization[4]:

$$\min(\sum_{i=1}^{8}(f_i - f_i^{\text{calc}}(\vec{B}))^2 \tag{S.1}$$

where f_i^{calc} are the eight ESR frequencies calculated from the NV Hamiltonian at a magnetic field $\vec{B}$ [5]:

$$H = DS_Z^2 + \gamma \vec{B} \cdot \vec{S}. \tag{S.2}$$

Here, D is the zero-field splitting (2.87 GHz), $S_{\text{i=X,Y,Z}}$ are the Pauli spin-1 matrices, and γ is the electron gyromagnetic ratio (28 GHz/T). Capital XYZ denote the NV frame. The Z-axis is taken along the NV axis and thus differs for the four NV families, pointing along the unit vectors

$$\hat{n}_{\text{NV}} = \frac{1}{\sqrt{3}}(\pm 1, \pm 1, 1) \tag{S.3}$$

expressed in the lab/diamond frame. The microwave stripline is oriented along the [110] direction in this frame.

After fitting the eight ESR frequencies, $f_{i=1-8}$, (Fig. S.1a),we extract the magnetic field components (B_x, B_y, B_z) (Fig. S.1b), the magnetic-field magnitude B_0 and the corresponding out-of-plane angle, θ, and in-plane angle, φ (Fig. S.1c). Lowercase xyz refer to the lab frame.

The field is oriented in-plane up to 10 mT (see B_z, Fig S.1b), after which the out-of-plane component is increased such that the field matches the target NV axis at 30 mT (red dashed line in Fig. S.1c). This ensures a good f_- ESR contrast over the entire field range [6].

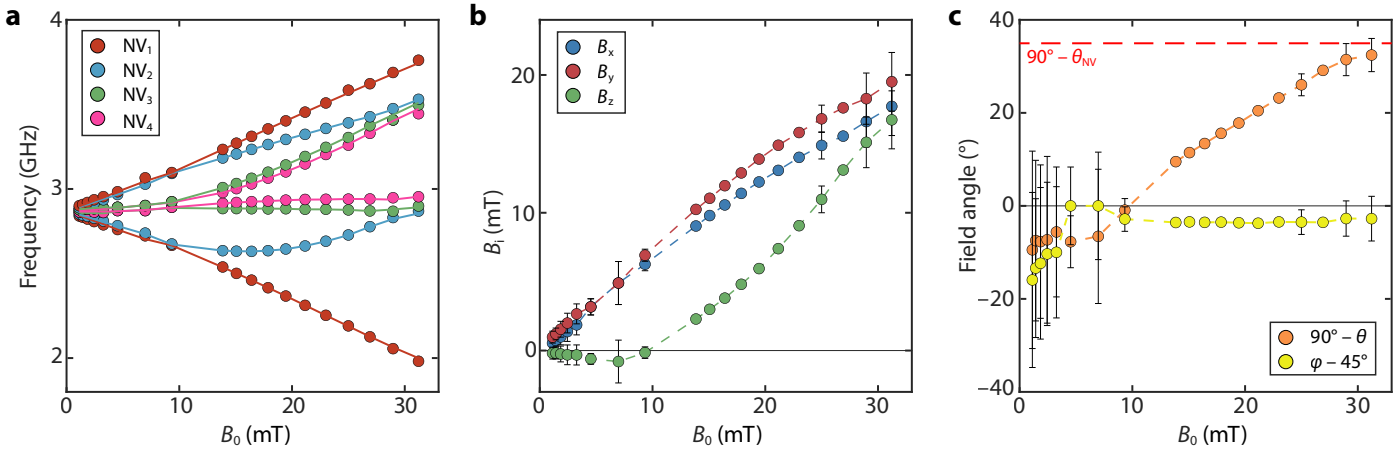

Figure S.1: Vector magnetic field determination. (a) The eight ESR frequencies as a function of applied external magnetic field (B_0). Filled circles: data. Solid lines: fitted ESR frequencies obtained by performing a least square minimization of Eq. (S.1) at each field. (b) The magnetic field components (B_x, B_y, B_z) as a function of the field magnitude B_0. The error bars represent 95% confidence bounds. (c) The magnetic field angles as a function of B_0. The error bars represent 95% confidence bounds.

5 NV relaxation induced by thermal magnons

We follow the approach of Rustagi et al.[7] to calculate the NV relaxation rates induced by the magnons in our YIG film, using

$$\Gamma_{\mp}(\omega_{\mp}) = \frac{\gamma^2}{2} \int \frac{d\vec{k}}{(2\pi)^2} \sum_{i,j \in \{x,y\}} \mathcal{D}_{\pm i}^{\text{eff}}(\vec{k}) \mathcal{D}_{\mp j}^{\text{eff}}(-\vec{k}) C_{ij}(\vec{k}, \omega_{\mp}). \tag{S.4}$$

[i] with 'NV family', we mean the collection of NV centers with the same crystallographic orientation

Here, $\Gamma_{\mp}$ are the relaxation rates corresponding to the $\omega_{\mp}$ ESR frequencies, $\vec{k}$ is the spin-wavevector, $\mathcal{C}$ is a spin-spin correlator describing the thermal magnon fluctuations, and $\mathcal{D}^{\text{eff}}$ is a dipolar tensor that calculates the magnetic stray fields that induce NV spin relaxation generated by these fluctuations. We will now summarize how these quantities are calculated for our measurement geometry. In addition, we will discuss the expected distance dependence of the relaxation rate that we compared with experiments in Fig. 4e of the main text.

The thermal transverse spin fluctuations in the film are described by [7]:

$$C_{ij}(\vec{k},\omega) = 2D_{th} \sum_{\nu=\{x,y\}} S_{i\nu}(\vec{k},\omega) S_{j\nu}(-\vec{k},-\omega) \tag{S.5}$$

where $D_{\text{th}} = \frac{\alpha k_B T}{\gamma M_s L}$, with k_B the Boltzmann constant, T the temperature, and

$$S(\vec{k},\omega) = \frac{\gamma}{\Lambda} \begin{bmatrix} \omega_3 - i\alpha\omega & -\omega_1 - i\omega \\ -\omega_1 + i\omega & \omega_2 - i\alpha\omega \end{bmatrix} \tag{S.6}$$

is the spin-wave susceptibility, with[7]

$$\omega_0(\vec{k}) = \omega_{\text{B}} \cos(\theta_0 - \theta) - \omega_{\text{M}} \cos^2\theta_0 + \omega_D k^2, \tag{S.7}$$

$$\omega_1(\vec{k}) = \omega_{\text{M}} f_k \sin\phi_k \cos\phi_k \cos\theta_0, \tag{S.8}$$

$$\omega_2(\vec{k}) = \omega_0 + \omega_{\text{M}} \left[f_k \cos^2\phi_k \cos^2\theta_0 + (1 - f_k) \sin^2\theta_0 \right], \tag{S.9}$$

$$\omega_3(\vec{k}) = \omega_0 + \omega_{\text{M}} f_k \sin^2\phi_k, \tag{S.10}$$

$$\Lambda(\omega) = (\omega_2 - i\alpha\omega)(\omega_3 - i\alpha\omega) - \omega_1^2 - \omega^2. \tag{S.11}$$

Here, $f_k \equiv 1 - (1 - e^{-kL})/(kL)$ with L the film thickness, and ϕ_k is the polar angle of a spin wave in k-space. The spin-wave dispersion is obtained by taking the real part of the solutions of $\Lambda = 0$. To calculate S we use $L = 235 \pm 10$ nm, Gilbert damping $\alpha = (1.2 \pm 0.1) \cdot 10^{-4}$, $M_s = (1.42 \pm 0.01) \cdot 10^5$ A/m [8] and $A_{\text{ex}} = (3.7 \pm 0.4) \cdot 10^{-12}$ J/m [9]. The equilibrium angle of the magnetization θ_0 is obtained by finding the minimum of the free energy at each value of the magnetic field (θ_0 is in-plane to within a few degrees for the field range used in our measurements).

The dipolar tensor $D^{\text{eff}}(\vec{k},\omega)$ calculates the magnetic stray fields that induce NV spin relaxation generated by the thermal magnons in the film. Because the correlator C is expressed in the frame of the magnet (with a z-axis pointing along the equilibrium magnetization), $D^{\text{eff}}(\vec{k},\omega)$ is obtained by first rotating the magnet frame to the lab frame, then multiplying by the dipolar tensor $\mathcal{D}(\vec{k})$ in the lab frame, and then rotating the result to the NV frame: $D^{\text{eff}}(\vec{k},\omega) = R_{yz}(\theta_{\text{NV}}, \phi_{\text{NV}}) \mathcal{D}(\vec{k}) R_Y(\theta_0)^T$, where

$$\mathcal{D}(\vec{k}) = -\frac{\mu_0 M_s}{2} e^{-|\vec{k}| d_{\text{NV}}} (1 - e^{-|\vec{k}|L}) \begin{bmatrix} \cos^2\phi_k & \sin(2\phi_k)/2 & i\cos\phi_k \\ \sin(2\phi_k)/2 & \sin^2\phi_k & i\sin\phi_k \\ i\cos\phi_k & i\sin\phi_k & -1 \end{bmatrix}, \tag{S.12}$$

where μ_0 is the vacuum permeability and d_{NV} is the distance between the NV and the sample surface. The terms in Eq. (S.4) that induce spin relaxation are given by[7]: $\mathcal{D}^{\text{eff}}_{\pm\nu} = \mathcal{D}^{\text{eff}}_{x\nu} \pm i\mathcal{D}^{\text{eff}}_{y\nu}$.

For a magnon gas in thermal equilibrium, in the absence of microwave driving, the dependence of the NV relaxation rate on the NV-sample distance can be calculated using Eq. (S.4). We find a good match between the calculated and measured rate (Fig. 4e main text) if we include an offset distance of 0.28 ± 0.03 µm. This offset distance is larger than the 20 nm NV implantation depth, which could be caused by small particles picked up by the tip during scanning. We observe a similarly fast decay over a broad range of magnetic field values (Fig. S.2).

6 Extracting the NV relaxation rate

In this section, we describe how we obtain the relaxation rate of a target NV family, plotted in Figs. 3 and 4 of the main text[i]. To extract the Γ_- relaxation rate of the target NV family we apply the pulse sequence shown in Fig. 3b of the main text. We perform two sequences: without and with a microwave π-pulse on the $|0\rangle \leftrightarrow |-1\rangle$ ESR transition of the target NV family. For the measurement without a π-pulse, we write the photoluminescence collected during readout as:

$$N(t) = p_0(t) N_0 + p_{-1}(t) N_{-1} + p_{+1}(t) N_{+1} + N_{\text{BG}} \tag{S.13}$$

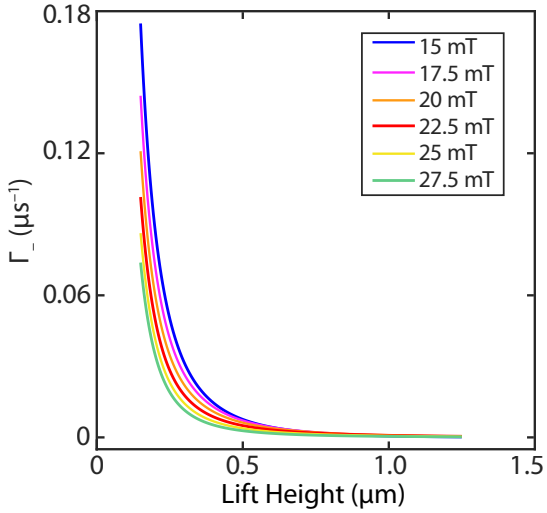

Figure S.2: Calculated relaxation rate as a function of tip lift height for an in-equilibrium occupation of the spin-wave band for different magnetic fields. We used $\theta_{\mathrm{NV}} = 54.7°$ and field-angle $\theta = 71.7°$ with respect to the surface normal.

where $N_{i=-1,0,+1}$ are the number of collected photons when the target NVs are in state i and $p_{i=-1,0,+1}$ are the associated occupation probabilities. N_{BG} is the background PL, which includes the contribution of the other NV families.

Applying a π-pulse on the $|0\rangle \leftrightarrow |-1\rangle$ transition of the target NV family switches the populations of these states. The photoluminescence collected during readout now is

$$N_\pi(t) = p_{-1}(t)N_0 + p_0(t)N_{-1} + p_{+1}(t)N_{+1} + N_{\mathrm{BG}}. \tag{S.14}$$

By taking the difference of equations (S.13) and (S.14), the background contribution drops out, giving

$$N - N_\pi = (p_0(t) - p_1(t))(N_0 - N_{-1}). \tag{S.15}$$

For the field range used in our experiments $\Gamma_+ \ll \Gamma_-$ [7] because the ω_+ transition is far detuned from the FMR and moreover less affected by the fields produced by the spin waves in the YIG film. As such, the time dependence of $N - N_\pi$ is dominated by the Γ_- relaxation rate and follows an exponential decay $N - N_\pi = Ae^{-2\Gamma_- t}$ that we use to extract Γ_-.

References

(1) Appel, P.; Neu, E.; Ganzhorn, M.; Barfuss, A.; Batzer, M.; Gratz, M.; Tschöpe, A.; Maletinsky, P. Fabrication of all diamond scanning probes for nanoscale magnetometry. *Review of Scientific Instruments* **2016**, *87*, 063703.

(2) Maletinsky, P.; Hong, S.; Grinolds, M. S.; Hausmann, B.; Lukin, M. D.; Walsworth, R. L.; Loncar, M.; Yacoby, A. A robust scanning diamond sensor for nanoscale imaging with single nitrogen-vacancy centres. *Nature Nanotechnology* **2012**, *7*, 320–324.

(3) Ruf, M.; IJspeert, M.; Van Dam, S.; De Jong, N.; Van Den Berg, H.; Evers, G.; Hanson, R. Optically coherent nitrogen-vacancy centers in micrometer-thin etched diamond membranes. *Nano Letters* **2019**, *19*, 3987–3992.

(4) Lillie, S. E.; Broadway, D. A.; Dontschuk, N.; Scholten, S. C.; Johnson, B. C.; Wolf, S.; Rachel, S.; Hollenberg, L. C.; Tetienne, J. P. Laser Modulation of Superconductivity in a Cryogenic Wide-field Nitrogen-Vacancy Microscope. *Nano Letters* **2020**, *20*, 1855–1861.

(5) Van der Sar, T.; Casola, F.; Walsworth, R.; Yacoby, A. Nanometre-scale probing of spin waves using single electron spins. *Nature Communications* **2015**, *6*, 7886.

(6) Tetienne, J. P.; Rondin, L.; Spinicelli, P.; Chipaux, M.; Debuisschert, T.; Roch, J. F.; Jacques, V. Magnetic-field-dependent photodynamics of single NV defects in diamond: an application to qualitative all-optical magnetic imaging. *New Journal of Physics* **2012**, *14*, 103033.

(7) Rustagi, A.; Bertelli, I.; Van Der Sar, T.; Upadhyaya, P. Sensing chiral magnetic noise via quantum impurity relaxometry. *Physical Review B* **2020**, *102*, 220403.

(8) Bertelli, I.; Carmiggelt, J. J.; Yu, T.; Simon, B. G.; Pothoven, C. C.; Bauer, G. E.; Blanter, Y. M.; Aarts, J.; Van Der Sar, T. Magnetic resonance imaging of spin-wave transport and interference in a magnetic insulator. *Science Advances* **2020**, *6*, eabd3556.

(9) Klingler, S.; Chumak, A. V.; Mewes, T.; Khodadadi, B.; Mewes, C.; Dubs, C.; Surzhenko, O.; Hillebrands, B.; Conca, A. Measurements of the exchange stiffness of YIG films using broadband ferromagnetic resonance techniques. *Journal of Physics D: Applied Physics* **2014**, *48*, 015001.